frontiers | Frontiers in Earth Science

TYPE Original Research
PUBLISHED 12 January 2023
DOI 10.3389/feart.2022.1024357

OPEN ACCESS

EDITED BY
Jianhua Zhao,
China University of Petroleum, China

REVIEWED BY
Li Tian,
China University of Geosciences Wuhan, China
Shipeng Huang,
Research Institute of Petroleum Exploration and Development (RIPED), China

*CORRESPONDENCE
Xiaodong Guan,
guanxd@sinopec.com

SPECIALTY SECTION
This article was submitted to Geochemistry, a section of the journal Frontiers in Earth Science

RECEIVED 21 August 2022
ACCEPTED 31 October 2022
PUBLISHED 12 January 2023

CITATION
Wang L, Guan X, Wang J, Sun Z and Xu H (2023), Characteristics and controlling factors of the Upper Permian Dalong Formation in northwestern Sichuan Basin, China.
Front. Earth Sci. 10:1024357.
doi: 10.3389/feart.2022.1024357

Characteristics and controlling factors of the Upper Permian Dalong Formation in northwestern Sichuan Basin, China

Lu Wang[1,2], Xiaodong Guan[3]*, Jianyong Wang[4], Zuoyu Sun[1] and Huiyuan Xu[2]

[1]School of Earth and Space Sciences, Peking University, Beijing, China, [2]State Key Laboratory of Shale Oil and Gas Enrichment Mechanisms and Effective Development, Beijing, China, [3]Department of science and Technology Development, Sinopec, Beijing, China, [4]Department of Oilfield Exploration and Production, Sinopec, Beijing, China

It has been generally accepted that the Permian shale is an important target for shale oil and gas exploration. In order to precisely predict the distribution of potential excellent source rocks of shale oil and gas, it is necessary to reveal the forming process and mechanism of high-quality source rocks, such as the Dalong Formation in the Scihuan Basin. In this study, 17 samples were collected from the Dalong Formation in Longfeng Quarry, Northwest Guangyuan City, Sichuan Province. The lithofacies, organic geochemistry, and pyrolysis of these samples were analyzed to evaluate the main factors controllingthe source rock formation. In particular, the influences of hydrothermal and paleoenvironmental conditions on the accumulation of organic matter were analyzed. The total organic carbon (TOC) content of the samples, which ranges from 0.05% to 12.21%, is closely related to the lithology. High TOC has been generally observed in rock intervals developed in a deep-water sedimentary environment, including siliceous rock, dark shale, and siliceous shale. The peak pyrolysis temperature of the samples ranges from 444°C to 462°C, indicating a mature stage. Thin-section observation, combined with the results of previous studies, has confirmed that the source of the organic matter is mainly marine phytoplankton, such as algae and radiolarians, ostracods, and other marine organisms, which consist of these high-quality source rocks. The ratio of trace elements, such as Ni/Co, V/Cr, U/Th, and V/(V + Ni) indicate that high-quality source rocks are mainly formed in anoxic restricted environments. The hydrothermal activity of submarine volcanoes provided many nutrients and compounds, resulting biological prosperity and improving primary productivity. This is simultaneously conducive to the formation of anoxic environments and the preservation of organic matter.

KEYWORDS

sichuan basin, paleoenvironment, trace elements, hydrocarbon source rocks, hydrothermal effects, organic-inorganic interaction

1 Introduction

Shale gas is an important unconventional natural gas, and its commercial production in some countries has attracted worldwide attention. The United States describes shale gas revolution as "a revolution that can change the world's energy pattern" (Curtis and Montgomery, 2002; Bowker, 2007). Since the commencement of shale gas revolution in the United States in 2010, China's fundamental research and industrial development of shale gas have been developing gradually; and many sets of organic-rich black shales have been developed in China (Nie et al., 2011; Zou et al., 2016; Mei et al., 2022). According to many predictions from different institutes, shale gas resources amount up to 83.3–134.4 × 10^{12} m^3, and of which 10.0–36.1 × 10^{12} m^3 are economical recoverable in China.

Recently, the drilling depth of oil and gas exploration in the northern Sichuan Basin has reached 7000 m, and confirmed that the Dalong Formation has a huge oil and gas potential (Dong et al., 2015). Previous studies conducted on the Dalong Formation found that the total organic carbon (TOC) was very high, and silicalite and mudstone in the Dalong Formation contained good types of organic matter, making it a set of high-quality marine source rocks (Chen et al., 2012; Shao et al., 2016; Liu et al., 2017; Peng et al., 2021; Xiao et al., 2021).

Previous studies have also evaluated the distribution characteristics of organic matter and its hydrocarbon generation potential of the Dalong Formation (Guo et al., 2016; Qiao et al., 2016; Dai et al., 2018; Li et al., 2019). However, the preservation and rock formation conditions are poorly understood (Xia et al., 2010; Yin et al., 2012; Yin and Song, 2013; Wei et al., 2018a; Wei et al., 2018b). To this end, this study conducted petrographic, organic geochemical, and pyrolysis analyses on the Dalong Formation samples collected from the Longfeng Quarry in Northwest Township, Guangyuan, the Sichuan Basin. The controlling factors on the forming of the Dalong Formation to be source rock, particularly the influence of hydrothermal action and paleosedimentary environment on the accumulation of organic matter, were investigated.

2 Geological background

Located in northwest of the Yangtze Platform, the large sedimentary Sichuan Basin covers a rhombic-shaped area of approximately18 × 10^4 km^2 (Figure 1A). Surrounded by high mountains, the basin is divided into three major districts. The east one is a low mountain with an altitude of 250–1000 m, the west one is a plain, and the middle one is a hill with an altitude of −250–750 m (Mingyi et al., 2012; Wei et al., 2018a). The Sichuan Basin, as an extremely important onshore gas-producing area in China, has been affected by multiperiod, superimposed structural changes since the Sinian Period. During the Sinian, the Sichuan Basin was a large-scale depression, into which a thick purple-red sandstone shale was deposited during the Mesozoic (Xie et al., 2007; Yin et al., 2012; Xie et al., 2017), making an overlying thick marine Sinian-Middle Triassic interval up to −3000–6000 m. Main sedimentary interval in the Sichuan Basin, of which neritic carbonate platforms are dominant, with marine and continental interfacies containing coal measures and terrigenous clasts (Jin et al., 2000; Liu et al., 2018; Liu et al., 2019a). The source rocks, which are widely distributed organic-rich shale, were developed in the main strata and considered to be the source of natural gas in many large- and medium-sized gas fields in Permian-to Triassic-aged strata.

The Guangyuan area within the study area is located at the intersection of the Dabashan fold belt and the Longmenshan fault belt (Figure 1B). The Changxing, Dalong, and Feixianguan Formations are successive deposits on the profile taken in the Longfeng Quarry, Northwest Township, Guangyuan. Observation of the field outcrop indicates that there is a −5-m-thick light-gray limestone containing layered flint nodules in the Permian Changxing Formation underlying the Dalong Formation, and in whose upper part there is a −50-cm-thick light-gray layered flint-nodule limestone.

The lower part of the Dalong Formation (Figure 2A) is composed of, from the bottom to the top, thick-layered gray-black siliceous rock; thin-layered gray-white volcanic ash; thin-layered gray-black siliceous rock; thin-layered gray-black siliceous rock with lamellar siliceous shale; middle-layered siliceous limestone; thin-layered gray-black platy siliceous shale; middle-layered dark-gray siliceous limestone with interbeds of thin-layered gray-black siliceous shale; thick-layered light-gray limestone; and middle-layered gray-black siliceous with thin-layered siliceous shale.

The middle part of the Dalong Formation (Figure 2B) is composed of, from the bottom to the top, thin-layered gray-black siliceous shale; middle-layered light-gray limestone whose top and bottom are gray-black siliceous rock interbedded with thin siliceous shale; thin-layered gray-white tuff; gray-black medium-to thin-layered siliceous rock with thin-layered gray-white volcanic ash 0.7 m from the bottom; middle-layered gray-black siliceous limestone; thin-layered gray-black siliceous rock containing asphalt; middle-layered gray-black siliceous rock; thin-layered gray-black siliceous rock; and middle-layered gray-black siliceous rock with bituminous at the top; middle-layered gray-black siliceous shale sandwiched with a limestone 2.0 × 0.8 m lens (Figure 2C); medium-to thin-layered gray-black siliceous rock containing numerous ammonite fossils up to a maximum diameter of 8 cm and containing asphalt.

The upper part of the Dalong Formation (Figure 2D) is composed of middle-layered dark-gray siliceous limestone interlayered with layered siliceous limestone and thin (3 cm) volcanic ash (the siliceous limestone becomes thick upward); middle-layered gray-white limestone and thin-layered dark-gray siliceous limestone interbeds with thin siliceous shale containing

double-shell fossils; thin-layered light-yellow tuff whose surface is weathered to gray-white and blue-gray middle-layered nodular argillaceous limestone with purple tumor-like protrusion on the surface, and numerous ammonite fossils. The Feixianguan Formation, located near the Dalong Formation, contains light-gray middle tuff intercalated with carbonate nodules in an upward sequence. The surface of the nodules is oxidized to purple-red, and the middle-thin blue-gray nodular limestone is intercalated with middle light-gray (30 cm thick) limestone. The surface is fractured and contains limestone concretions, light-gray middle-thick lamellar marl, and light-gray middle-thick limestone.

Various types of biota were observed in the Dalong Formation, including algae, calcispheres, ostracods, gastropods, foraminifera, crinoids, ammonites, brachiopods, radiolarians, and conodonts (Xie et al., 2017). Few flints occur in layered siliceous rocks. In addition to pyrite, fossilized foraminifera, phytoplankton, ammonite siliceous radiolarians and thin bivalves, were observed. Some calcareous bioshells have been intensely silicified. Radiolarians, mainly concentrated in the lower part of the Dalong Formation, are fragmented and difficult to identify. Algae exhibit detrital and leaf-like morphologies. Calcium globules are mainly round to oval, with the highest content in the middle, but less in both ends.

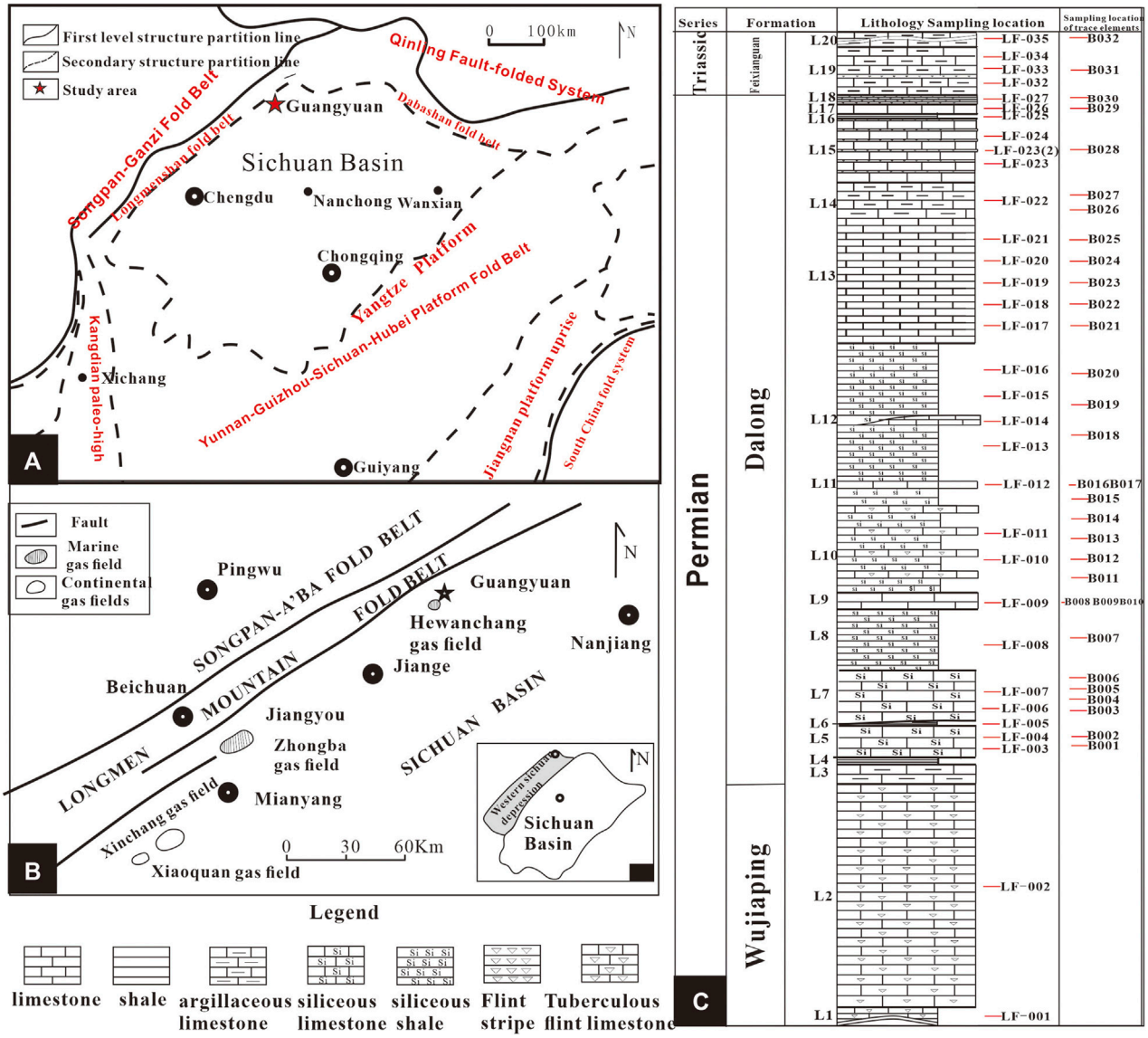

FIGURE 1
Geographical map of Sichuan Basin and sampling location **(A)** Geographical map of the Sichuan Basin. **(B)** Distribution of gas fields in the Sichuan Basin. **(C)** Lithological column of the Dalong Formation in Guangyuan and this study's sampling locations.

Ostracods, concentrated in the lower to middle sections, are thick shelled and mostly fragmented. Gastropods are mainly snails, particularly in the middle section, and they are well preserved. Foraminifera organisms are mostly concentrated in the upper section. Crinoids appear in the middle section, and there are many ammonite fossils that can be observed in the outcrops, mainly in the middle and upper sections (Xiao et al., 2017; Xie et al., 2017).

The role of episodic volcanic or intrusive magmatic activity in triggering global-scale perturbations during the Early Triassic, the ~5-million-year interval following the latest Permian mass extinction (LPME) is suspected but has not been strongly evidenced to date. Shen et al.(2019) investigate the record of volcanism through the Early Triassic (with a focus on the Smithian-Spathian Boundary, or SSB) using mercury (Hg) concentrations in marine sediments as a proxy. Shen et al.(2010) reported Late Permian igneous rocks in the Dalong Formation, Guangyuan. Similarly, this study found three layers of volcanic ash, confirming the occurrence of volcanic activities in the Dalong Formation.

3 Experimental methods

3.1 Samples

Rock samples were obtained from the Longfeng Quarry, Northwest Township, Guangyuan, the Sichuan Basin. The sampling interval was −50 cm. The sampling locations are shown in Figure 1C, and the test methods are listed in Table 1. 14 samples were selected for pyrolysis to analyze TOC and total sulfur (TS); 24 samples were selected for making thin-sections; 12 samples were analyzed for trace elements; 2 samples were analyzed for major elements; and 4 samples were tested for biomarker compounds.

3.2 Test methods

The pollution-free fragmentation and major element testing of whole-rock samples were undertaken at the Institute of Geology and Geophysics, Chinese Academy of Sciences (Beijing, China). Specifically, the rock samples were coarsely crushed, washed, and dried. The samples were subsequently crushed to <8 mm with a nonpolluting agate crusher, placed in the agate tank of a nonpolluting agate ball mill, and ground to <200 mesh for X-ray fluorescence spectrometry.

A Gas chromatography-mass spectrometry (GC-MS) was employed (HP 5890 II; Hewlett Packard). Trace element analysis was performed in the State Key Laboratory of Biogeology and Environmental Geology, China University of Geosciences (Wuhan, China). Trace element analysis was performed by inductively coupled plasma-mass spectrometry (ICP-MS). Approximately 50 mg of powdered sample was accurately weighed, ground to 200 mesh, and placed in a Teflon crucible. The sample was subsequently wetted with 1–2 drops of high-

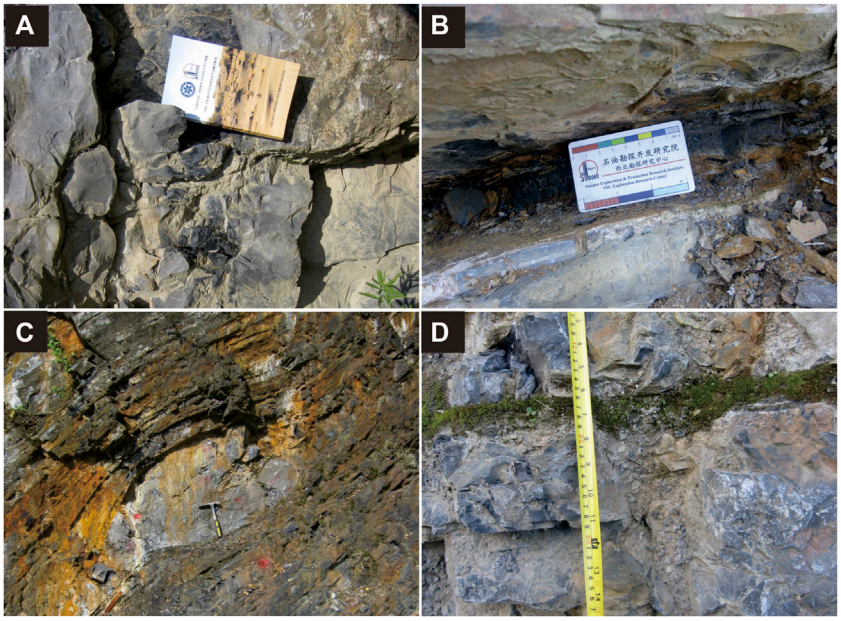

FIGURE 2
Field outcrops in the study area **(A)** Thick-layered gray-black siliceous rock. **(B)** Thin-layered gray-black siliceous shale. **(C)**Middle-layered gray-black siliceous shale sandwiched with a limestone 2.0 m × 0.8 m lens. **(D)** Middle-layered dark-gray siliceous limestone.

TABLE 1 Pyrolysis parameters of the source rocks of the Dalong Formation from Longfeng Quarry, Northwest Township, Guangyuan.

	S1 (mg/g)	S2 (mg/g)	Tmax (°C)	S1+S2 (mg/g)	TOC (%)	PI	HI (mg/g)	PC (%)	D (%)	HC (mg/g)
LF-001	0.02	0.03	462	0.05	0.05	0.40	54.67	0.00	0.00	36.45
LF-003	3.42	15.59	449	19.01	11.68	0.18	133.48	1.58	13.53	29.28
LF-004	2.03	6.44	447	8.47	8.28	0.24	77.82	0.70	8.46	24.53
LF-006	2.81	14.55	448	17.36	5.75	0.16	252.87	1.44	25.03	48.84
LF-007	0.08	0.16	454	0.24	12.21	0.33	1.31	0.02	0.16	0.66
LF-008	1.66	8.72	447	10.38	9.78	0.16	89.14	0.86	8.79	16.97
LF-009	0.02	0.03	552	0.05	0.13	0.40	22.64	0.00	0.00	15.09
LF-010	3.63	13.54	445	17.17	4.02	0.21	336.98	1.43	35.59	90.34
LF-011	0.92	3.77	444	4.69	6.62	0.20	56.99	0.39	5.90	13.91
LF-013	1.28	5.81	449	7.09	4.96	0.18	117.09	0.59	11.89	25.80
LF-016	1.10	6.94	449	8.04	4.57	0.14	151.99	0.67	14.67	24.09
LF-018	0.93	3.10	452	4.03	3.49	0.23	88.93	0.33	9.47	26.68
LF-019	0.36	1.41	459	1.77	1.10	0.20	127.83	0.15	13.60	32.64
LF-020	0.50	4.06	452	4.56	3.88	0.11	104.67	0.38	9.80	12.89

S_1, soluble hydrocarbon; S_2, pyrolytic hydrocarbon; Tmax, temperature of maximum rate of pyrolysis; TOC, total organic carbon; PI, production index (S1/[s1 + s2]); HI, hydrogen index; PC, available carbon; D, degradation rate; HC = (S1 × 100)/TOC.

purity water, 1 ml of HNO_3 and 1 ml of HF were added successively, and the sample was placed in an open Teflon beaker. The Teflon crucible was placed in a tightly-screwed steel jacket and put into an oven at 195°C for over 48 h. After the dissolving bomb was cooled and the acid completely evaporated, the lid was opened, and the sample was placed on an electric hot plate (115°C) to evaporate to dry. Thereafter, 1 ml of HNO_3 was added, and the sample was evaporated to dry again. During this process, we ensured that there was no liquid on the wall of the Teflon crucible. If black suspended matter was present, 1–2 drops of $HClO_4$ were added after evaporating to dry, and the sample was evaporated to dry again. After this, 3 ml of 30% HNO_3 was added, and the Teflon crucible was placed in a steel jacket, tightened, placed in an oven, and heated to 195°C for over 12 h. The solution was subsequently transferred into a polyethylene vial, diluted with 2% HNO_3 to −100 g, and stored under airtight conditions in preparation for ICP time-of-flight MS. To determine the analytical precision and the precision of trace element data, GBW07105 (GSR-3) was used as the standard. Each sample was analyzed three times, and the final average result was used. The analytical precision of the trace elements was estimated to be 5%. A total of 35 elements were detected in the solid samples using the high-temperature and high-pressure closed digestion method.

TOC and TS were tested at China University of Petroleum (Beijing). After treatment with 10% hydrochloric acid to remove carbonates, the samples were subjected to TOC and TS analysis using a carbon/sulfur analyzer (CS-344; LECO) with analytical precision of ±0.1%. The samples were ground to 80–100 mesh and extracted with chloroform for 72 h. After distilling the solvent, the asphalt fraction was separated by petroleum ether precipitation, and the aliphatic and aromatic fractions were eluted by n-hexane, benzene, and ethanol silica gel-alumina column chromatography and resin fractions.

The biomarker compounds were tested at the Massachusetts Institute of Technology (Massachusetts, United States). All the samples were decontaminated, pulverized to powders, and extracted with dichloromethane. The extracts were separated into paraffinic, aromatic, and polar component paraffinic fractions using silica gel chromatography for GC (gas chromatography) and C-C-MS (Capillary gas chromatography-mass spectrometry) analysis. The compounds

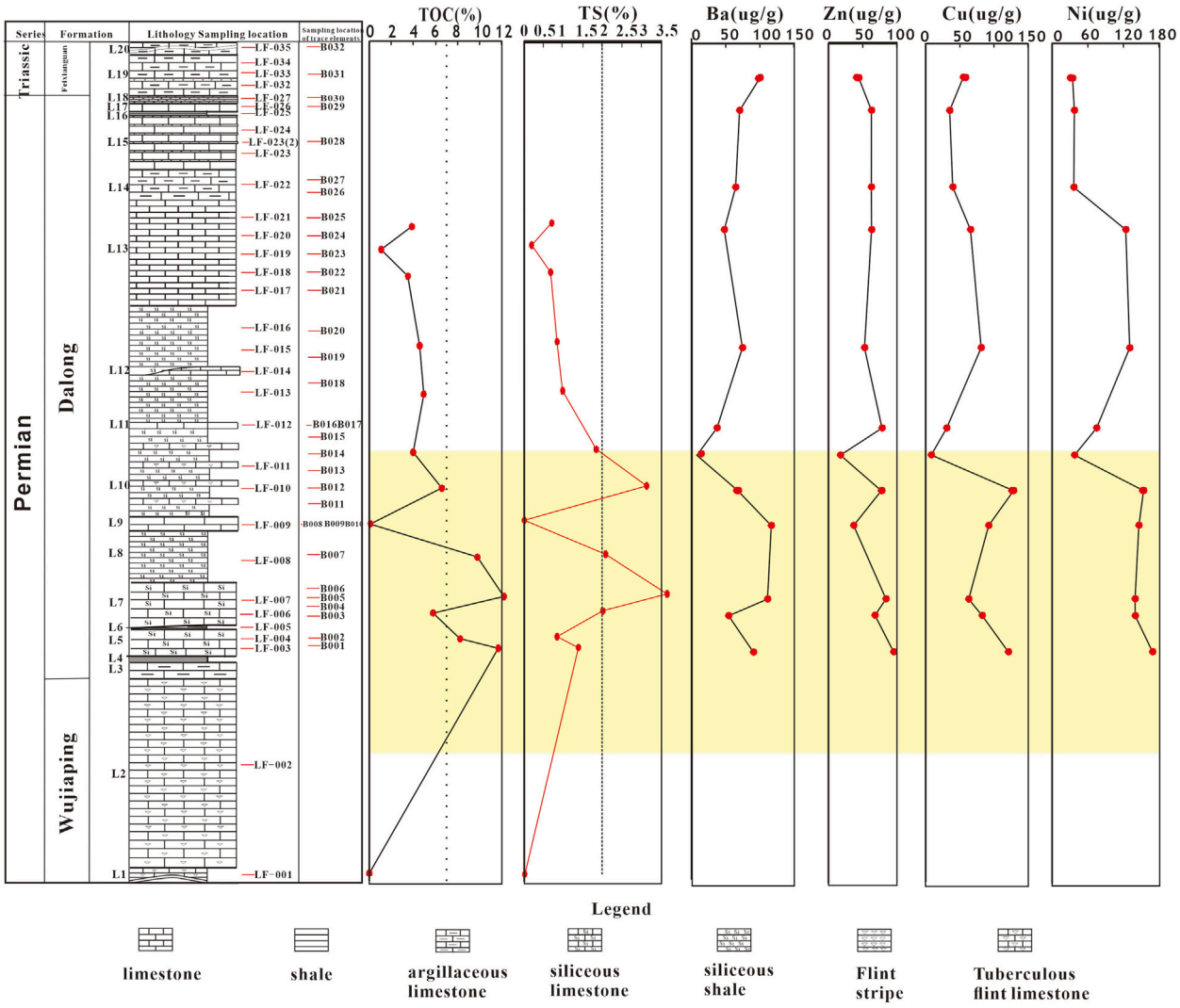

FIGURE 3
Vertical trends in TOC, redox indicators, and paleoproductivity proxies of the Dalong Formation. TS, total sulfur.

were identified by comparison with standard chromatograms. The n-alkane parameters were calculated based on the m/z 85 mass chromatogram, and the hopane series compounds were calculated based on the m/z 191 mass chromatogram.

4 Results

4.1 Abundance of organic matter

The results of the organic geochemical test are presented in Table 1.

The TOC of 14 of the Permian Dalong Formation samples was analyzed. To study the changes in the TOC of the mudstone/limestone or mudstone/siliceous rocks (mudstone or marl) in certain interbeds, individual samples of thin and lenticular layers, such as strips or thin layers within the limestone layers, were collected. The TOC results are presented in Figure 3; Table 1. The TOC varies from 0.05% to 12.21%, with an average of 5.62% and a maximum of 12.21% in layer 7.

First, the TOC is closely related to the lithology of the host (siliceous shale). As shown in Figure 3; Table 1, the TOC varies significantly: the TOC in the bioclastic siliceous shale generally exceeds 10%; the TOC of the siliceous shale with no or extremely little bioclastic material is generally between 4.5% and 9%; and the TOC of the bioclastic limestone is extremely low, at only 0.13%. The TOC of thick limestone in the Changxing Formation is only 0.05%. Second, there is a relationship between the TOC

and the layer thickness. In the Dalong Formation, the TOC in the thick limestone is generally lower than 0.5%. However, in the corresponding layered or siliceous marl, the TOC exceeds 4%. Generally, the thickness of the limestone layer is inversely proportional to the TOC (i.e., the thinner the limestone layer, the greater the TOC). More organic matters accumulate in the layered mudstone and thin limestone.

The hydrogen index (HI) of the Dalong Formation source rocks ranges from 1.31 to 336.98 mg/g, with an average of 115.46 mg/g. Their hydrocarbon generation potential is between 0.05 and 19.01 mg/g, with an average of 7.35 mg/g. The hydrocarbon generation potential was roughly at two peaks: 19.01 mg/g and 17.07 mg/g, corresponding to samples LF-003 and LF-010, respectively. In addition, in general, the hydrocarbon generation potential of the lower Dalong Formation source rock is greater. The available carbon (PC) of the Dalong Formation exhibits a similar double-peak shaped distribution. The two peaks, 1.58 and 1.43, correspond to samples LF-003 and LF-010, respectively. The PC of the source rock in the lower part of the Dalong Formation is higher, indicating that the lower part of the Dalong Formation contains high-potential hydrocarbon-generating organic carbon. The histogram for each S1/TOC interval shows that LF-010 has the largest value (0.90), indicating that the proportion of potential soluble hydrocarbons in the TOC still exceeds that of LF-010.

4.2 Total sulfur

TS in the Upper Permian Dalong Formation shale ranges between 0.01% and 3.65%, with an average of 1.26%, a maximum of 3.65% in layer 7, and a minimum of 0.01% in layer 1, as shown in Table 1. In layer 9, a minimum TS of 0.03% was found with a minimum TOC. The bioclastic siliceous shale (siliceous mudstone) has a high TS content, while the thick bioclastic limestone (thick siliceous limestone) has a low TS content. Figure 3 shows that TS and TOC are roughly positively correlated with each other. It has also confirmed that the rock formation with the highest TOC has a high TS content, which indicates that the rock formation with the highest TOC may undergo a high degree of reduction.

4.3 Source of organic matter

Thin sections of the organic matter indicate that the lower part of the Dalong Formation comprises bioclastic siliceous shale (Figure 4A), microcrystalline limestone, and weakly silicified, interbedded bioclast-bearing carbonaceous mudstone containing ostracods, radiolarians, and calcium globules. Subhorizontal and discontinuous carbonaceous shale laminae were observed, and local asphaltization was observed in fractures. Carbonaceous shale, calcium spheres (Figure 4B), and bioclastic limestone as well as weak silicification were observed in the middle part of the Dalong Formation. Many types of organisms were observed inside the calcium spheres, such as foraminifera, brachiopod, ostracod, and gastropod (Figure 4C). It was speculated that a siliceous calcium sphere in the mudstone was a siliceous radiolarian (Figure 4D). The top part of the Dalong Formation comprises micrite limestone, bioclastic micrite limestone, silicified carbonaceous and shaly calcium spheres, and micrite limestone with horizontal bedding and containing algal debris and radiolarians. A few of the samples contain asphalt, and yellow iron ore in the siliceous rocks, along with less flint. In addition, pyrite and fossils of foraminifera and phytoplankton, such as ammonites, siliceous radiolarians, and thin bivalves, were observed. In the siliceous radiolarian mudstone, some radiolarians were filled with organic matter to varying degrees (Figure 4E).

Biomarker compounds can be used to infer the source of organic matter, such as terrestrial or marine and algae, bacteria, or higher plants (Xiao et al., 2017). (Xiaoyan et al., 2008).confirmed the predominance of low-molecular-weight n-alkanes in the Upper Permian Dalong Formation, leading to the speculation that the origin of the marine organic matter in the Dalong Formation in Shangsi, Guangyuan, was mainly from algae and bacteria. Wei et al. (2018b) found that the C_{12}^{+} n-alkanes in the Dalong Formation shale are mainly nonwaxy congeners, which are typical marine organisms produced by local phytoplankton. Herein, the results of standard biological compounds tested in samples LF-006, LF-008, LF-011, and LF-013 (Figure 5A) led to the speculation that the source of the organic matter was mainly lower aquatic organisms, bacteria, and algae.

We analyzed the source of the organic matter (i.e., the type of kerogen) according to the cross-plot of Tmax and HI (Figure 5B). Most of the organic matters belong to types II_1-II_2, namely sapropel, which is common in source rocks. This type of sapropel is mainly derived from bacteria and phytoplankton in catchment basins and has a high hydrocarbon generation potential of −0.3–0.5.

4.4 Thermal maturity

Tmax can be used as an indicator of maturity. As shown in Figure 5B, most samples have Ro in the range of 0.8–1.2, indicating a high-maturity stage. The Tmax values of the samples, presented in Table 2, range from 444°C to 462°C, except for sample LF-009, where the Tmax value is 552°C. Sample LF-009 is bioclastic limestone with a TOC of 0.3%. It is not a source rock, so it is not discussed further herein. Therefore, the organic-rich Dalong Formation in Longfeng Quarry is at a high-maturity stage.

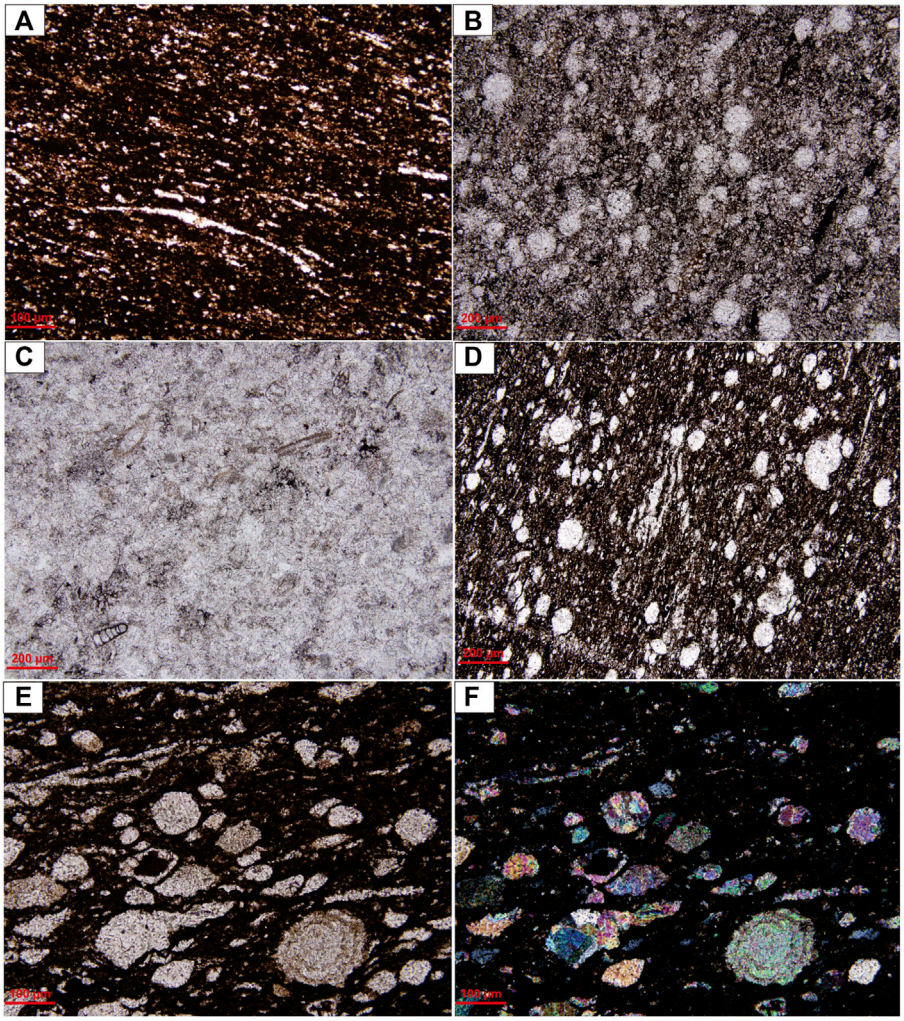

FIGURE 4
Lithological microscopic photos of the Dalong Formation. **(A)** Bioclastic siliceous shale, biodetritus aligned in a directional manner. **(B)** Calcium spheres, the calcium spheres are not uniform in size. **(C)** Bioclastic limestone, such as foraminifera, brachiopod, ostracod, and gastropod. **(D)** Radiolarian, and **(E)** Spherules filled with organic matter by polarizing microscope with plane polarized light. **(F)** spherules filled with organic matter by polarizing microscope with perpendicular polarized light.

5 Discussion

5.1 Controlling factors on high-quality source rocks

Many factors control the formation of high-quality source rocks, including productivity, the effect of the depositional environment on the preservation of organic matter, and hydrothermal activity (Song et al., 2016; Song et al., 2019; Meng et al., 2022). We studied the sedimentary paleoenvironment and the hydrothermal activity associated with the Dalong Formation high-quality source rocks.

5.1.1 Paleoenvironment for source rock deposition

In black shale, metal elements combine with sulfide and organic matter through symbiotic mineralization. Factors affecting the content of metal elements include redox conditions, organic matter type, deposition rate, diagenesis, and subsequent mineralization. Previous studies have shown that certain metals exhibit high fluxes and mobilities under anoxic conditions, leading to a significant enrichment of these metals in sediments (Meng et al., 2013). Therefore, organic-rich sediments are usually enriched with sulfide metal elements through redox reactions. The trace elements in the Dalong Formation samples are presented in Table 2. Several

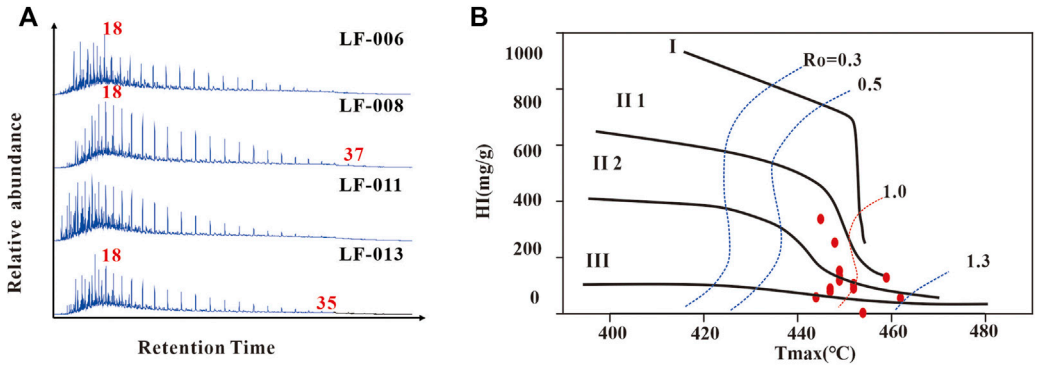

FIGURE 5
Analysis of the source of the organic matter in Dalong Formation. **(A)** Normal alkane distribution of the source rocks, and **(B)** crossplot of Tmax with HI of the source rocks.

trace elements, including Mo, Re, U, and V, are regarded as signs of hypoxia in paleosedimentary environments. The ratios of certain trace elements, such as V/(V + Ni), V/Cr, Ni/Co, and U/Th, indicate reducing conditions to restore the depositional environment. Reduction-sensitive trace elements, such as Mo, U, and V, are enriched in anoxic environments, rendering element concentrations and ratios useful indicators for paleoreduction reconstructions.

Previous studies have observed that V/(V + Ni), V/Cr, Ni/Co, and U/Th can be used to indicate ancient redox environments (Wei et al., 2018b). Although there is no consensus among these redox indicators, Ni/Co, V/Cr, U/Th, and V/(V + Ni) show an overall downward trend with increasing water oxidation· Previous studies have established standard values for Ni/Co, V/Cr, U/Th, and V/(V + Ni) ratios to distinguish oxygen-rich, oxygen-poor, and anoxic conditions (Francois, 1988). Therefore, using the sample test data, the standard values for various Ni/Co, V/Cr, U/Th, and V/(V + Ni) ratios were used to distinguish oxygen-rich, oxygen-poor, and anoxic conditions, as shown in Figure 6. Generally, samples B002, B004, B006, B008, B013, B015, B016, B018, and B021 from the middle and lower sections of the Dalong Formation are within the hypoxia-hypoxia region, while samples B026, B029, and B031 from the top of the Dalong and Feixianguan Formations are within the oxygen-enriched region. Therefore, we speculated that the organic matter in the lower part of the Dalong Formation was mainly deposited under semianoxic to anoxic conditions, while the top of the Dalong Formation was deposited in an oxygen-rich environment. This is consistent with the sedimentary history of the Permian. In the Early Permian, transgression occurred in the Sichuan Basin, and at the end of the Permian, the Sichuan Basin experienced regression. It was then entirely uplifted, denuded, and remained under oxygen-rich conditions. Therefore, the Early Permian is significantly different from the Late Permian.

The Ni/Co, V/Cr, and U/Th ratios strongly correlate with TOC (Figure 7). Peaks were observed at L7 and L10, and the values were higher in the middle and lower sections of the Dalong Formation. However, the values were lower at the top of the Permian Dalong and Triassic Feixianguan Formations. Thus, it's confirmed that the rock layers with high TOC (i.e., the rock layers with abundant organic matter) are related to the preservation conditions for organic matter.

High-resolution biomarker profiles from Shangsi can help to identify the succession of environmental and related microbial community changes that occurred during the PTB (Permian-Triassic boundary) crisis. Xie et al. (2017) reveal major differences in the microbial communities and environmental conditions by biomarker records. The first episode of the PTB mass extinction was probably associated with massive soil erosion ($C_{30}M/C_{30}HP$ >0.20; Pr/Ph >2), expansion of oceanic anoxia (r/C_{30} HP >0.1), and blooms of marine red algae (C_{27}/C_{27-29} sterane ratio >0.4) and nitrogen-fixing bacteria (C_{31} 2-MHP >0.05, decrease in $\delta^{15}N_{org}$). The Pr/Ph ratio is frequently used to judge redox conditions (Chen et al., 2012). A Pr/Ph value of <1 indicates an anoxic environment. When the value is between 1 and 3, it indicates a subanoxic environment. When the value is >3, it indicates that the organic debris was deposited in a full-oxygen terrestrial environment. Figure 5A shows the distribution of n-alkanes in Longfeng Quarry samples. The Pr/Ph ratio of the Dalong Formation high-quality source rocks ranges from 0.8 to 1.0, so we speculate that their depositional environment may have been anoxic. The DBT/P shown in Figure 8A represents depositional environments. The depositional environments of samples LF-006, LF-011, and LF-013 were similar, while the depositional environment represented by sample LF-008 was more reduced. Figure 8 presents the biological compound spectra of samples LF-006, LF-008, LF-011, and LF-013 and shows (A) the m/z 178 + 184 distribution and (B) aromatic distribution characteristics of the samples.

As shown in Figure 8B, in four samples LF-006, LF-008, LF-011 and LF-013, the abundance of dimethylnaphthalene is similar, while

TABLE 2 Trace elements (μg/g) of the source rocks of Dalong and Changxing formations in northwestern Sichuan basin.

Samples	B002	B004	B006	B008	B013	B015	B015	B016	B018	B021	B026	B029	B031-2	B031-2
Be	2.29	1.09	1.63	1.28	0.23	0.9	0.85	0.23	0.82	0.94	0.63	0.88	1.37	1.27
Sc	7.33	5.49	6.45	4.68	1.45	6.11	6.08	1.43	4.24	3.76	3.43	6.97	8.62	8.35
V	309	403	1112	972	128	1136	1116	287	581	1130	37	34.8	48.7	47.2
Cr	190	169	216	350	15.8	132	138	78.4	169	173	22.2	53.9	40.3	42.4
Co	15.3	14.7	20.7	21.4	4.7	18.8	18.7	60.5	21.7	12.9	12.3	16.3	16.7	19.2
Ni	169	140	138	146	37.6	152	154	75.4	131	124	35.8	37.3	30	32.5
Cu	121	63.2	82.9	92.3	7.51	129	126	30.5	80.5	64.9	38.8	34.8	52.9	56.3
Zn	95.1	83.7	68.2	37.2	17.6	77.2	77.9	23.7	52.6	62.9	38	53.5	44.3	41
Ga	8.72	4.96	7.05	7.73	0.38	4.62	4.45	1.68	4.69	3.93	3.62	5.69	9.21	8.76
Rb	42.1	20.2	47.4	40.3	1.6	34.4	34.6	7.06	22.5	25.9	20.7	40.2	59.1	57.9
Sr	883	1575	359	71.4	467	1520	1512	243	721	372	2995	702	539	514
Y	15.4	50.4	11.3	5.32	4.08	28.6	28.4	8.4	13.3	11.2	6.91	9.09	17.3	16.8
Zr	76.4	65	68.9	57.2	8.33	48	47.5	25.6	37.9	33.1	35.4	39.6	73.3	68.9
Nb	15	4.68	8.06	6.12	0.63	4.79	4.68	1.42	3.11	3.05	2.93	4.07	7.38	7.14
Cs	2.42	1.07	2.52	2.33	0.06	1.63	1.6	0.58	1.51	1.33	1.28	2.28	3.4	3.25
Ba	89.8	54.4	111	117	7.59	67.4	66.3	37.2	73.9	47.3	64.7	70.7	99.7	95
La	13.3	48.3	14.2	7.81	2.71	23	22.6	6.99	13.4	8.27	7.81	10.9	22.4	21.4
Ce	17.6	60.4	25	12.1	3.43	34.4	33.8	11.9	22.7	14.8	14.6	21.8	41.7	40.3
Pr	2.49	7.29	3.24	1.51	0.46	4.91	4.77	1.64	3	1.85	1.65	2.43	5.02	4.8
Nd	9.12	27.2	12.1	5.15	1.75	18.8	18.2	6.47	11.1	7.22	6.05	9.11	18.9	18.1
Sm	1.63	5.32	2.09	0.77	0.35	4.07	4.03	1.35	2.02	1.53	1.18	1.79	3.59	3.49
Eu	0.32	0.98	0.35	0.16	0.07	0.72	0.7	0.2	0.34	0.29	0.22	0.3	0.68	0.67
Gd	1.68	6.08	1.76	0.7	0.38	4.27	4.29	1.33	2.13	1.59	1.2	1.62	3.49	3.39
Tb	0.3	1.02	0.29	0.12	0.07	0.73	0.73	0.24	0.37	0.27	0.19	0.27	0.55	0.53
Dy	1.85	5.96	1.59	0.71	0.41	4.16	4.13	1.37	2.04	1.6	1.07	1.5	2.95	2.85
Ho	0.42	1.25	0.34	0.17	0.10	0.84	0.83	0.28	0.43	0.34	0.23	0.31	0.58	0.55
Er	1.46	3.78	1.11	0.62	0.3	2.42	2.35	0.83	1.27	1.02	0.66	0.9	1.66	1.63
Tm	0.26	0.56	0.2	0.12	0.05	0.35	0.35	0.14	0.21	0.16	0.1	0.14	0.26	0.24
Yb	1.83	3.24	1.3	0.87	0.34	2.16	2.1	0.9	1.37	1.04	0.68	0.94	1.55	1.53
Lu	0.3	0.51	0.21	0.15	0.06	0.34	0.33	0.14	0.21	0.16	0.11	0.14	0.23	0.23
Hf	1.76	1.05	1.68	1.44	0.16	1.18	1.16	0.42	1.19	0.84	0.95	1.1	2.03	1.9
Ta	0.47	0.26	0.54	0.4	0.05	0.31	0.29	0.17	0.44	0.24	0.23	0.3	0.54	0.53
Pb	10.6	7.25	12.1	8.2	1.36	15.5	15.2	3.8	9.12	8.63	69.6	12.2	9.57	9.24
Th	4.19	2.21	5.39	3.24	0.44	3.24	3.18	0.84	10.8	2.75	2.24	3.49	6.19	5.94
U	5.68	29.7	6.98	5.95	8.53	19	18.8	5.78	12.5	22.6	6.38	3.8	2.27	2.17

the abundance of 1,2,5-trimethylnaphthalene is different, indicating that the source rocks were affected by biogenesis, particularly the influence of low microbial activities or the input of higher plants. The 2-/1-methylphenanthrene parameters indicate the similar maturity of all the samples.

5.2 Hydrothermal influence

South China as a whole was likely covered frequently by felsic ash beds around the PTB time. 21 fine-grained tuff beds of centimeter scale occer in the 12-m-thick PTB interval. These indicate that rhyodacitic volcanism was active, and that northern Sichuan often experienced ash falls at the end of the Permian. This implies that the eruptions of felsic volcanoes may have played a certain role in environmental change relevant to the mass extinction at the end of Permian (Isozaki et al., 2007). Direct evidence of intense chemical weathering induced by volcanism is rare in sedimentary successions. Shen et al. undertake a multiproxy analysis (including organic carbon isotopes, mercury (Hg) concentrations and isotopes, chemical index of alteration (CIA), and clay minerals) of two well-dated Triassic-Jurassic (T-J) boundary sections. Both sections show increasing CIA in association with Hg peaks near the T-J boundary, reflecting volcanism-induced intensification of continental chemical

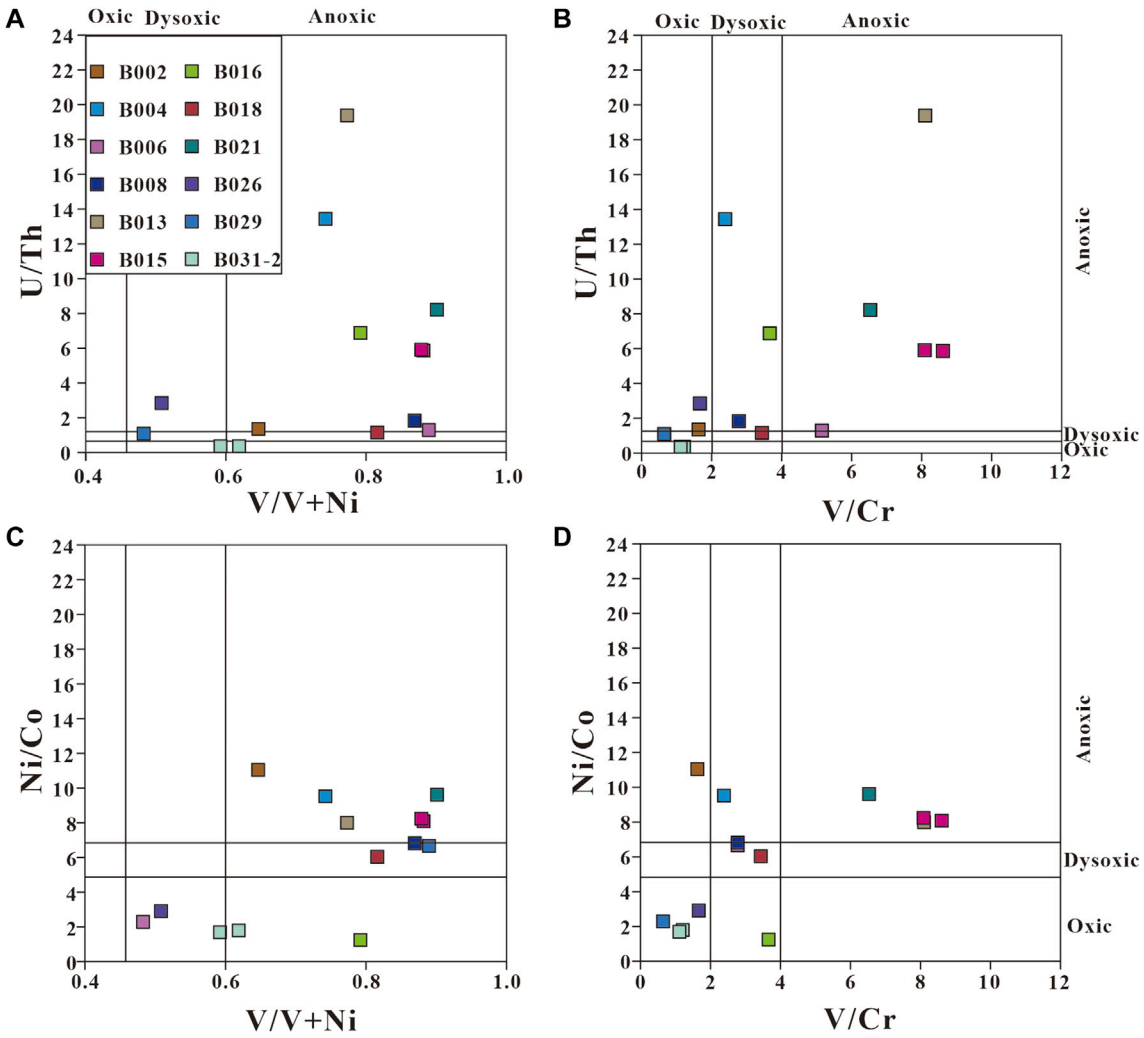

FIGURE 6
Crossplots of Ni/Co, V/Cr and U/Th ratios of samples of the Dalong Formation takin in Longfeng Quarry, Northwest Township, Guangyuan. **(A)** U/Th *vs.* V/(V + Ni). **(B)** U/Th *vs.* V/Cr. **(C)** Ni/Co *vs.* V/(V + Ni). **(D)** Ni/Co *vs.* V/Cr.

weathering, which is also supported by negative mass-independent fractionation (MIF) of odd Hg isotopes. (Shen et al., 2022).Three layers of 3–5 cm thick volcanic ash were observed in the field outcrops. Volcanic ash settled from the atmosphere into certain depositional environments can be transformed into altered rocks with a high clay mineral content through burial, diagenesis, and metamorphism (Meng et al., 2013; Meng et al., 2022). The volcanic ash deposits in the study area were grayish white in color and stick-slip after wetting with water, and they exhibited heavy alteration (Shen et al., 2022). Two relatively fresh volcanic ash samples were selected for major elemental analysis and testing. The test data are shown in Table 3.

The SiO_2 content ranges from 49.34% to 56.46%, Al_2O_3 from 22.91% to 22.93%, K_2O + Na_2O from 4.23% to 4.435%, and MgO from 1.47% to 2.67% which differs by ±3.5% compared to normal igneous rock. The TiO_2/Al_2O_3 ratio ranges from 0.014 to 0.015, which is lower than the upper limit of igneous rocks (0.02), and the SiO_2/Al_2O_3 ratio ranges from 2.15 to 2.46. All these values indicate a high clay mineral content, high maturity, and heavily altered volcanic ash sediments. According to previous studies, the enrichment of nutrient elements such as Ni, Cu, Zn, Ba, and Cd in carbonate rocks indicates high paleoproductivity, and the enrichment of Ni/Co, V/Cr, U/Th, and other elements indicates reducing conditions (Francois, 1988). Similar trends in the abundance maps of Ni, Cu, Zn, Ba, and TOC indicate that they were affected to a similar degree by environmental factors (Figure 2). The trends in Ni, Cu, Zn and Ba, and elemental Ni/Co, V/Cr, and U/Th ratios (which represent a redox environment) are also similar. A peak was observed for the Ni/Co, V/Cr, and U/Th ratios. We speculate that the aggregation of the nutrient elements Ni, Cu, Zn, and Ba was related to the redox conditions, whereby they

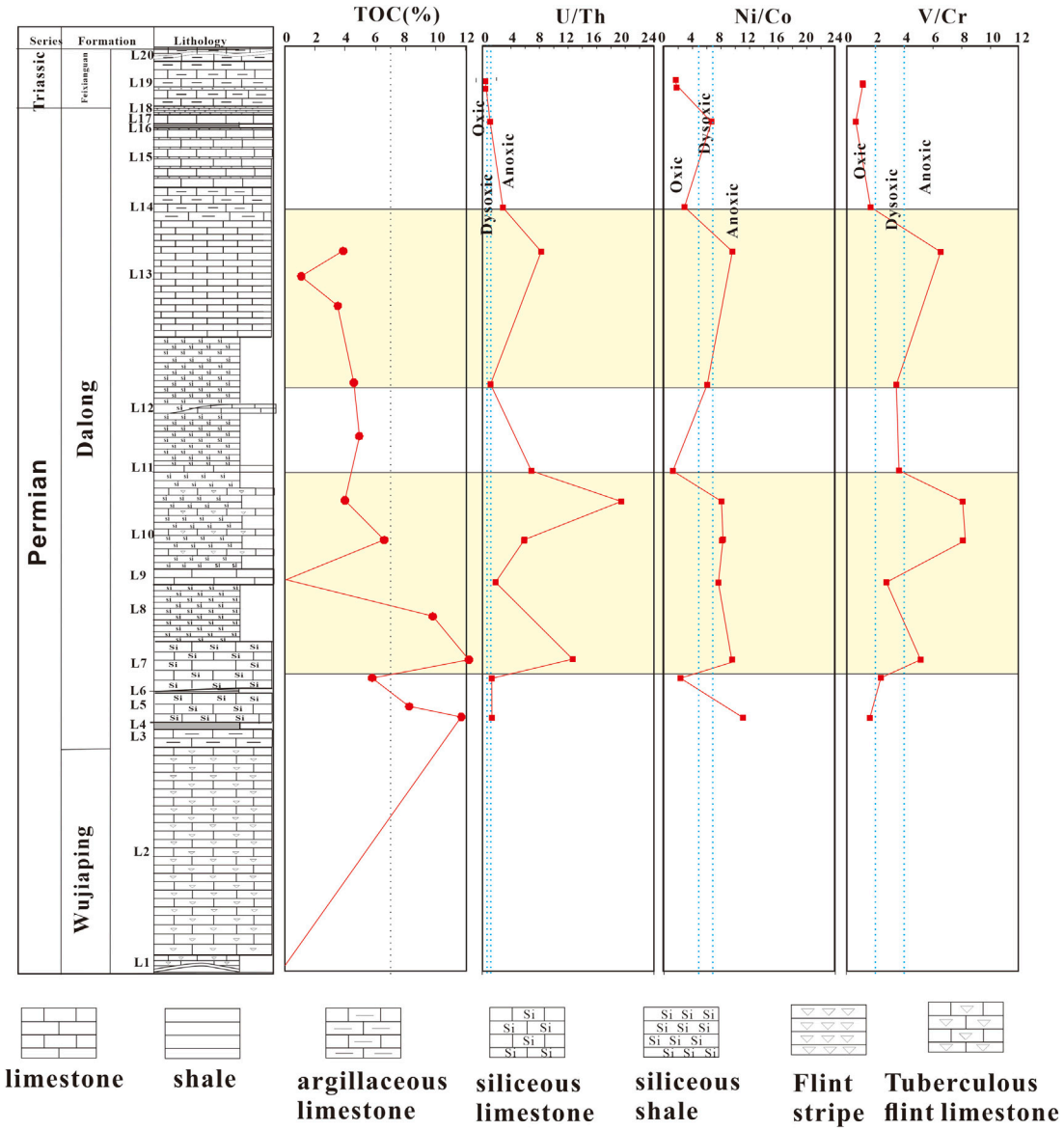

FIGURE 7
Variation in TOC, Ni/Co, V/Cr, and U/Th ratios of samples taken in Longfeng Quarry in Northwest Township, Guangyuan.

aggregated under reducing conditions. Considering that these nutrients, particularly Ba, represent ancient productivity, we speculate that the level of ancient productivity was also related to redox conditions. The nutritional elements Ni, Cu, Zn, and Ba strongly correlate with the TOC, and the redox indices, Ni/Co, V/Cr, and U/Th, show a good relationship with the TOC, reflecting that the accumulation of TOC may be affected by the level of paleoproductivity and paleo-redox conditions. There are evidences of strong control and influence from reducing conditions.

Many Upper Permian Dalong Formation sedimentary rocks with high TOC were developed at low slopes and basin bottoms. However, the sediments dominated by limestone at the top of the Changxing and Dalong Formations have obviously low TOC. Moreover, three layers of volcanic ash were observed in the field outcrops. As shown in the geochemical test data, the layers of siliceous rock and shale with high TOC were affected by hydrothermal activities. So it is inferred that high paleoproductivity has taken place in these rock layers. To elucidate the relationship between hydrothermal activity and accumulation of organic matter, we propose the following concept. The process of submarine volcanic hydrothermal activity is associated with abundant nutrients such as Mo, Pb, Ni, Zn, Ba, Sb, and P (Liu et al., 2019b; Liao et al., 2019; Li et al., 2020; Shen et al., 2022).

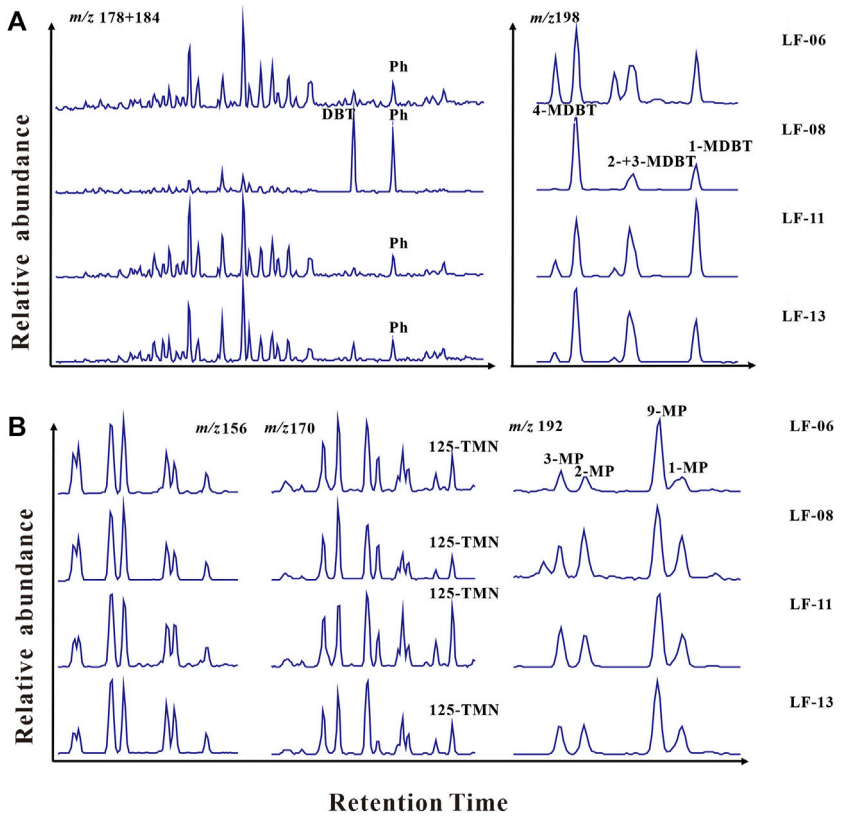

FIGURE 8
Standard biological compounds of samples 2018-LF-006, 2018-LF-008, 2018-LF-011, and 2018-LF-013. **(A)** Distribution of m/z 178 + 184, and **(B)** aromatic distribution.

TABLE 3 Major Elements of volcanic ash sedimentary rocks in Longfeng Quarry, Northwest Township, Guangyuan (Wt%).

samples	SiO_2	TiO_2	Al_2O_3	TFe_2O_3	MnO	MgO	CaO	Na_2O	K_2O	P_2O_5	LOI	TOTAL
LF-25	56.46	0.327	22.93	1.28	0.01	1.47	3.99	0.175	4.26	0.17	8.95	100.02
LF-5	49.34	0.354	22.91	5.42	0.02	2.67	1.85	0.07	4.16	0.136	12.61	99.54

In this case, the solubility of these elements rapidly increases with increasing water temperature. When Si-rich hot water meets cold seawater, Si may precipitate directly. As a result, siliceous and other biological organisms may thrive in hydrothermal environments. Biological prosperity leads to high primary productivity. However, flourishing organisms consume a large amount of free oxygen from the water, causing anoxic hypoxia in the bottom water. As the organic matter is buried deeper and deeper, anaerobic and anoxic conditions mainly control the accumulation of organic matter in the sedimentary and early diagenetic stages, providing important conditions for the preservation of organic matter in siliceous and dark shale. Therefore, we propose the following for the formation of the shale and siliceous rocks of the Upper Permian Dalong Formation in Longfeng Quarry. With submarine volcanic activities and hydrothermal (hot water) events, the paleoproductivity increased and the burial environment became reducing. In general, hydrothermal events and upwelling caused biological flourishing in the upper water body by providing nutrients, leading to an increase in primary productivity. Post-flourishing living processes consumed large amounts of free oxygen from the water, leading to the reduction of the burial conditions associated with microbial blooms at the bottom. These processes were one after the other and closely linked, and ultimately resulted in the burial of large amounts of organic matter in reducing environments that favored the formation of high-quality source rocks.

6 Conclusion

Based on microscopic observations, TOC, TS and trace element testing and analysis of shale samples from the Upper Permian Dalong Formation in Longfeng Quarry, Northwest Township, Guangyuan, the Sichuan Basin, and considering previous studies, we have the following conclusions.

The source rocks in the middle and lower members of the Dalong Formation are of high quality, and the TOC of the samples is closely related to the lithology. High TOC was tested in siliceous rock, dark shale and siliceous shale that were developed in a deep-water basin environment. In addition, high TOC is associated with the thickness of the rock layer. Generally, thinner layers have high TOC.

The Tmax-HI diagram shows that the organic matter sources are mainly types II1 and II2. The biomarker compounds and microscopic observation show that the main sources of organic matter are phytoplankton and bacteria. The Tmax values of the source rocks range from 444°C to 462°C, and the corresponding Ro is roughly 1.0%–1.5%, indicating the high-maturity stage.

The TS, V content, and trace element ratios (i.e., Ni/Co, V/Cr, U/Th, and V/[V + Ni]) indicate deposition in a closed/anoxic environment, and Pr/Ph = 0.8–1.0 also proves the depositional environment is closed and under anoxic conditions.

Submarine volcanic hydrothermal activity provides abundant nutrients and compounds, such as SiO_2, Al_2O_3, K_2O, Mo, Pb, Ni, Zn, Ba, Sb, and P, which contribute to biological prosperity and high primary productivity. This consumes large amounts of free oxygen from the water, and results in inadequate oxygen in the bottom water and better preservation of organic matter in siliceous rock and dark shale. This is conducive to the formation of high-quality source rocks.

Data availability statement

The original contributions presented in the study are included in the article/supplementary material, further inquiries can be directed to the corresponding author.

Author contributions

LW: Conceptualization, Methodology, Formal ananlysis, Data curation, Writing—original draft, Visualization. XG: Conceptualization, Writing—review, Resources, Funding acquisition, WJ: Data curation, Writing; ZS: Writing—review HX: Data curation.

Funding

This study was supported by National Scientific Funding of China (Grant No.U20B6001 and 41872164), National Key Research and Development Program (Grant No. 2019YFA0708504).

Acknowledgments

We are grateful to Meng Qingqiang for the guidance of this article, CX for assistance with the biomarker compounds operation at the Massachusetts Institute of Technology; Ding Baoming for assistance with the major element testing of whole-rock samples. The authors would like to thank to the State Key Laboratory of Biogeology and Environmental Geology, China University of Geosciences (Wuhan, China).

Conflict of interest

The authors declare that the research was conducted in the absence of any commercial or financial relationships that could be construed as a potential conflict of interest.

Publisher's note

All claims expressed in this article are solely those of the authors and do not necessarily represent those of their affiliated organizations, or those of the publisher, the editors and the reviewers. Any product that may be evaluated in this article, or claim that may be made by its manufacturer, is not guaranteed or endorsed by the publisher.

References

Bowker, K. A. (2007). Barnett shale gas production, fort worth basin: Issues and discussion. *Am. Assoc. Pet. Geol. Bull.* 91, 523–533. doi:10.1306/06190606018

Chen, H., Xie, X., Hu, C., Huang, J., and Li, H. (2012). Geochemical characteristics of late permian sediments in the Dalong Formation of the Shangsi section, northwest Sichuan basin in south China: Implications for organic carbon-rich siliceous rocks formation. *J. Geochem. Explor.* 112, 35–53. doi:10.1016/j.gexplo.2011.06.011

Curtis, J. B., and Montgomery, S. L. (2002). Recoverable natural gas resource of the United States: Summary of recent estimates. *AAPG Bull.* 86, 1671–1678.

Dai, J., Yunyan, N. I., Qin, S., Huang, S., and Han, W. (2018). Geochemical characteristics of ultra-deep natural gas in the Sichuan Basin. *SW China* 45, 619–628.

Dong, D., Gao, S., Huang, J., Guan, Q., Wang, S., and Wang, Y. (2015). Discussion on the exploration & development prospect of shale gas in the Sichuan Basin. *Nat. Gas. Ind. B* 2, 9–23. doi:10.1016/j.ngib.2015.02.002

Francois, R. (1988). A study on the regulation of the concentrations of some trace metals (Rb, Sr, Zn, Pb, Cu, V, Cr, Ni, Mn and Mo) in Saanich Inlet Sediments, British Columbia, Canada. *Mar. Geol.* 83, 285–308. doi:10.1016/0025-3227(88)90063-1

Guo, C., Li, G., Wei, H., Xia, F., and Xie, F. J. a. J. O. G. (2016)., 9. China, 359. doi:10.1007/s12517-016-2348-3Stratigraphic architecture and platform evolution of the Changxing formation (upper permian) in the yuanba gas field, northeastern Sichuan basin, China*Arab. J. Geosci.*

Isozaki, Y., Shimizu, N., Yao, J., Ji, Z., and Matsuda, T. (2007). End-Permian extinction and volcanism-induced environmental stress: The Permian-Triassic boundary interval of lower-slope facies at Chaotian, South China. *Palaeogeogr. Palaeoclimatol. Palaeoecol.* 252, 218–238. doi:10.1016/j.palaeo.2006.11.051

Jin, Y. G., Wang, Y., Wang, W., Shang, Q. H., Cao, C. Q., and Erwin, D. H. (2000). Pattern of marine mass extinction near the Permian-Triassic boundary in South China. *Science* 289, 432–436. doi:10.1126/science.289.5478.432

Li, L., Liao, Z., Lei, L., Lash, G. G., Chen, A., and Tan, X. (2020). On the negative carbon isotope excursion across the wuchiapingian–changhsingian transition: A regional event in the lower Yangtze region, south China? *Palaeogeogr. Palaeoclimatol. Palaeoecol.* 540, 109501. doi:10.1016/j.palaeo.2019.109501

Li, Y., Chen, S., Wang, Y., Qiu, W., Su, K., He, Q., et al. (2019). The origin and source of the Devonian natural gas in the Northwestern Sichuan Basin, SW China. *J. Petroleum Sci. Eng.* 181, 106259. doi:10.1016/j.petrol.2019.106259

Liao, Z., Hu, W., Cao, J., Wang, X., Hu, Z. J. M., and Geology, P. (2019). Petrologic and geochemical evidence for the formation of organic-rich siliceous rocks of the Late Permian Dalong Formation, Lower Yangtze region, southern China. *Mar. Petroleum Geol.* 103, 41–54. doi:10.1016/j.marpetgeo.2019.02.005

Liu, Q., Jin, Z., Bing, Z., Zhu, D., and Meng, Q. J. J. O. N. G. G. (2017)., 2. China, 81–97.Main factors for large accumulations of natural gas in the marine carbonate strata of the Eastern Sichuan Basin

Liu, Q., Jin, Z., Wang, X., Yi, J., Meng, Q., Wu, X., et al. (2018). Distinguishing kerogen and oil cracked shale gas using H, C-isotopic fractionation of alkane gases. *Mar. Petroleum Geol.* 91, 350–362. doi:10.1016/j.marpetgeo.2018.01.006

Liu, Q., Zhu, D., Jin, Z., Meng, Q., and Li, S. (2019a). Influence of volcanic activities on redox chemistry changes linked to the enhancement of the ancient Sinian source rocks in the Yangtze craton. *Precambrian Res.* 327, 1–13. doi:10.1016/j.precamres.2019.02.017

Liu, Q., Zhu, D., Meng, Q., Liu, J., Wu, X., Zhou, B., et al. (2019b). The scientific connotation of oil and gas formations under deep fluids and organic-inorganic interaction. *Sci. China Earth Sci.* 62, 507–528. doi:10.1007/s11430-018-9281-2

Mei, Y., Liu, W., Wang, J., and Bentley, Y. (2022). Shale gas development and regional economic growth: Evidence from Fuling, China. *Energy* 239, 122254. doi:10.1016/j.energy.2021.122254

Meng, Q., Pang, Q., Hu, G., Jin, Z., Zhu, D., Liu, J., et al. (2022). Rhyolitic ash promoting organic matter enrichment in a shallow carbonate platform: A case study of the maokou Formation in eastern Sichuan basin. *Front. Earth Sci. (Lausanne).* 10. doi:10.3389/feart.2022.879654

Meng, Q. Q., Zhu, D. Y., Hu, W. X., and Jin, Z. J. (2013). Dissolution-filling mechanism of atmospheric precipitation controlled by both thermodynamics and kinetics. *Sci. China Earth Sci.* 56, 2150–2159. doi:10.1007/s11430-013-4711-5

Mingyi, H., Zhonggui, H., Guoqi, W., Wei, Y., and Mancang, L. (2012). Sequence lithofacies paleogeography and reservoir potential of the maokou Formation in Sichuan basin. *Petroleum Explor. Dev.* 39, 51–61. doi:10.1016/s1876-3804(12)60014-7

Nie, H., He, F., and Bao, S. (2011). Peculiar geological characteristics of shale gas in China and its exploration countermeasures. *Nat. Gas. Ind.* 31, 111–116.

Peng, H., Yin, C., Zhong, Y., Yang, Y. M., Xu, L., Luo, Y., et al. (2021). A new scale shoal-forming model and natural gas exploration implications in Feixianguan Formation, northwestern Sichuan Basin, China. *Energy Explor. Exploitation* 39, 1857–1877. doi:10.1177/01445987211005219

Qiao, Z., Janson, X., Shen, A., Zheng, J., Zeng, H., Wang, X. J. M., et al. (2016). Lithofacies, architecture, and reservoir heterogeneity of tidal-dominated platform marginal oolitic shoal: An analogue of oolitic reservoirs of Lower Triassic Feixianguan Formation, Sichuan Basin, SW China. *Mar. Pet. Geol.* 76, 290–309. doi:10.1016/j.marpetgeo.2016.05.030

Shao, T., Cheng, N., and Song, M. (2016). Provenance and tectonic-paleogeographic evolution: Constraints from detrital zircon U-Pb ages of Late Triassic-Early Jurassic deposits in the northern Sichuan basin, central China. *J. Asian Earth Sci.* 127, 12–31. doi:10.1016/j.jseaes.2016.05.027

Shen, J., Algeo, T. J., Planavsky, N. J., Yu, J., Feng, Q., Song, H., et al. (2019). Mercury enrichments provide evidence of Early Triassic volcanism following the end-Permian mass extinction. *Earth-Science Rev.* 195, 191–212. doi:10.1016/j.earscirev.2019.05.010

Shen, J., Yin, R., Zhang, S., Algeo, T. J., Bottjer, D. J., Yu, J., et al. (2022). Intensified continental chemical weathering and carbon-cycle perturbations linked to volcanism during the Triassic-Jurassic transition. *Nat. Commun.* 13, 299. doi:10.1038/s41467-022-27965-x

Shen, S. Z., Zhu, M. Y., Wang, X. D., Li, G. X., Cao, C. Q., and Zhang, H. (2010). A comparison of the biological, geological events and environmental backgrounds between the Neoproterozoic-Cambrian and Permian-Triassic transitions. *Sci. China Earth Sci.* 53, 1873–1884. doi:10.1007/s11430-010-4092-y

Song, D. F., Wang, T. G., and Li, M. J. (2016). Geochemistry and possible origin of the hydrocarbons from wells Zhongshen1 and Zhongshen1C, Tazhong Uplift. *Sci. China Earth Sci.* 59, 840–850. doi:10.1007/s11430-015-5226-z

Song, D., Li, M., Shi, S., Han, Z., and Meng, B. (2019). Geochemistry and possible origin of crude oils from Bashituo oil field, Tarim Basin. *Am. Assoc. Pet. Geol. Bull.* 103, 973–995. doi:10.1306/10031817403

Wei, Z., Wang, Y., Wang, G., Sun, Z., and Xu, L. (2018a). Pore characterization of organic-rich late permian da-long Formation shale in the Sichuan basin, southwestern China. *Fuel* 211, 507–516. doi:10.1016/j.fuel.2017.09.068

Wei, Z., Wang, Y., Wang, G., Sun, Z., Zhang, T., Xu, L., et al. (2018b). Paleoenvironmental conditions of organic-rich upper permian Dalong Formation shale in the Sichuan basin, southwestern China. *Mar. Petroleum Geol.* 91, 152–162. doi:10.1016/j.marpetgeo.2017.12.003

Xia, M., Wen, L., Wang, Y., Hong, H., Fan, Y., and Wen, Y. (2010). High quality source rocks in trough facies of upper permian Dalong Formation, Sichuan basin. *Petroleum Explor. Dev.* 37, 654–662. doi:10.1016/s1876-3804(11)60002-5

Xiao, D., Cao, J., Luo, B., Tan, X., Xiao, W., He, Y., et al. (2021). Neoproterozoic postglacial paleoenvironment and hydrocarbon potential: A review and new insights from the Doushantuo Formation Sichuan basin, China. *Earth-Science Rev.* 212, 103453. doi:10.1016/j.earscirev.2020.103453

Xiao, Y., Suzuki, N., and He, W. (2017). Water depths of the latest Permian (Changhsingian) radiolarians estimated from correspondence analysis. *Earth-Science Rev.* 173, 141–158. doi:10.1016/j.earscirev.2017.08.012

Xiaoyan, R., Genming, L., Shouzhi, H., Feng, C., Si, S., Wenjun, W., et al. (2008). Molecular records of primary Producers and sedimentary environmental conditions of late permian rocks in Northeast sichuan, China. *J. China Univ. Geosciences* 19, 471–480. doi:10.1016/s1002-0705(08)60052-7

Xie, S., Algeo, T. J., Zhou, W., Ruan, X., Luo, G., Huang, J., et al. (2017). Contrasting microbial community changes during mass extinctions at the Middle/Late Permian and Permian/Triassic boundaries. *Earth Planet. Sci. Lett.* 460, 180–191. doi:10.1016/j.epsl.2016.12.015

Xie, S., Pancost, R. D., Huang, J., Wignall, P. B., Yu, J., Tang, X., et al. (2007). Changes in the global carbon cycle occurred as two episodes during the Permian-Triassic crisis. *Geol.* 35, 1083–1086. doi:10.1130/g24224a.1

Yin, H. F., and Song, H. J. (2013). Mass extinction and Pangea integration during the Paleozoic-Mesozoic transition. *Sci. China Earth Sci.* 56, 1791–1803. doi:10.1007/s11430-013-4624-3

Yin, H., Xie, S., Luo, G., Algeo, T. J., and Zhang, K. (2012). Two episodes of environmental change at the Permian-Triassic boundary of the GSSP section Meishan. *Earth-Science Rev.* 115, 163–172. doi:10.1016/j.earscirev.2012.08.006

Zou, C., Dong, D., Wang, Y., Li, X., Huang, J., Wang, S., et al. (2016). Shale gas in China: Characteristics, challenges and prospects (II). *Petroleum Explor. Dev.* 43, 182–196. doi:10.1016/s1876-3804(16)30022-2